Korean J. Chem. Eng., **28**(1), 308-313 (2011)
DOI: 10.1007/s11814-010-0341-1

Flow regime recognition in the spouted bed based on Hilbert-Huang transformation

Wang Chunhua, Zhong Zhaoping†, and Li Rui

School of Energy and Environment, Southeast University, Nanjing 211189, P. R. China
(*Received 7 May 2010 • accepted 2 June 2010*)

Abstract−Empirical mode decomposition has been used to decompose the pressure fluctuation signals in the spouted bed into several intrinsic mode functions, and these modes were transformed from the time domain into the frequency domain by Hilbert transformation. According to the characteristic parameters extracted from these modes, flow regimes were recognized by RBF neural network, and parameters in RBF neural network were optimized by adaptive genetic algorithm. The recognition accuracy of packed bed, spouted bed, bubbly fluidized bed and slugging bed can reach 90%, 85%, 85%, 95%, respectively.

Key words: Empirical Mode Decomposition, Hilbert Transformation, Flow Regimes, RBF Neural Network, Adaptive Genetic Algorithm

INTRODUCTION

The commonly used method to recognize the flow regimes in the spouted bed is based on visual observation through the transparent walls of columns operated at atmosphere temperature, but this method mainly has two disadvantages: (1) visual observation is too subjective, and different researchers may have different investigation results; and (2) visual observation is not possible in industrial scale equipment. So there is incentive to develop some objective methods to recognize the flow regimes [1,2].

It is widely proved that the analysis of pressure fluctuation signals can be used to recognize the flow regimes in multi-phase flow [3-5], so this method may be also suitable in the spouted bed [6-12]. However, classical time-frequency analysis methods such as fast Fourier transformation (FFT), power spectrum density (PSD) have some limitations: (1) classical time-frequency analysis can only give the global energy-frequency distributions and fail to reflect the details of signals; (2) the classical time-frequency analysis is easy to diffuse and truncate the signals' energy because it regards the harmonic signals as basic components; and (3) the central frequency of the filter is determined by experience, which has great subjective influence on the results. Because of these disadvantages, it is difficult to recognize the flow regimes in the spouted bed purely based on classical time-frequency analysis.

To break the limitation of the classical time-frequency analysis methods, the Hilbert-Huang transformation (HHT) is presented [13-16]. In this method, the original signals are firstly decomposed into many intrinsic mode functions (IMF), called empirical mode decomposition (EMD), and then Hilbert transformation (HT) is used to transform each mode from the time domain into the frequency domain. The frequency components contained in each IMF component not only relate to the sampling frequency but also change with the signals (in fact, the amplitude components also change with the signals). At present, HHT has been widely applied in fields such as ocean [17,18], multi-phase flow [19], machinery fault diagnosis [20, 21], and it is found HHT is more suitable for the analysis of nonlinear signals.

In this paper, HHT has been applied to the analysis of the pressure fluctuation signals in the spouted bed, and the energy extracted from each IMF component was used as the input vector of RBF neural network. The flow regimes in the spouted bed can be recognized by observing the output of an RBF neural network.

EXPERIMENTAL SYSTEM

The experimental system consists of a visible semi-cylindrical spouted bed column, a gas supply system and a multi-channel pressure signals sample system.

The column, which is made of 5 mm thick Plexiglas, is 0.1 m in diameter and 1.8 m in height. The diameter of spout nozzle is 10 mm. The conical base has an internal angle of 60°. An air compressor supplies the spouting gas, which is controlled by a pressure regulator and measured by rotor meter. The particles used in these experiments are quartz sands, and their physical characters are shown in Table 1. Pressure measuring holes are located on the back wall of the column at the height of 0.1 m, 0.24 m, 0.34 m, 0.44 m, and 0.54 m above the bottom of the bed (in this paper, only differential pressures between the hole at the height of 0.24 m and 0.44 m are measured). Pressure signals are logged into a computer via an A/D converter with 12-bit resolution; the sampling frequency used for each measurement is 600HZ, 1024 data points are sampled each time. 380 groups of signals are sampled at different spouting velocities in these experiments (300 groups of the signals are regarded as the train-

Table 1. Characters of particle used in these experiments

Material	Mean diameter, mm	Particle density, kg/m^3	Bulk density, kg/m^3	Voidage	Shape
Quartz sands	0.5	2560	1393	0.456	Spherical

†To whom correspondence should be addressed.
E-mail: Zzhong@seu.edu.cn

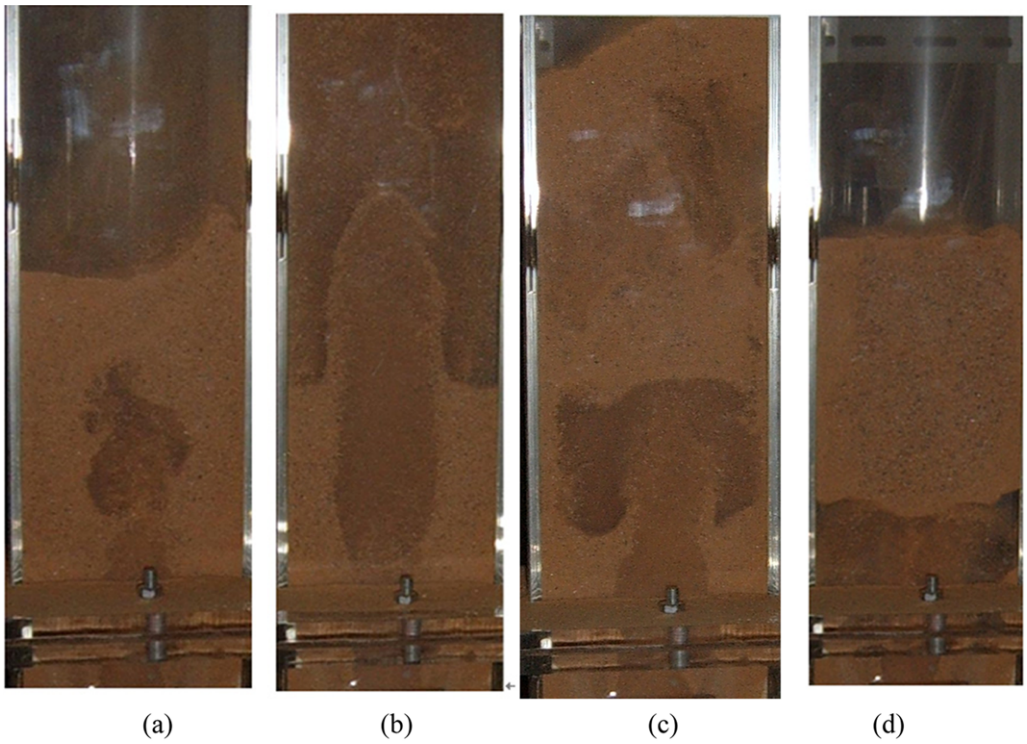

Fig. 1. Flow regimes in the spouted bed: (a) packed bed; (b) stable spouting; (c) bubbling fluidized bed; (d) slugging bed.

ing samples, and the residual are regarded as the testing samples).

In previous studies [22], the validity index was defined to evaluate the validity of fuzzy *c*-means clustering, and it was found that the index could reach its maximum when the clustering number equaled to 4. Accordingly, flow in the spouted bed could be classified into four kinds of flow regimes: packed bed (including internal jet), spouted bed, bubbling fluidized bed and slugging bed. So in this paper, packed bed (P), spouted bed (S), bubbling fluidized bed (BF) and slugging bed (SB) are recognized. The typical flow regimes are shown in Fig. 1.

HILBERT-HUANG TRANSFORMATION [13-17] OF THE PRESSURE FLUCTUATION SIGNALS

1. EMD Method

EMD is based on the simple assumption that any signals can be decomposed into a finite number of different simple intrinsic mode functions (IMF), and each mode should satisfy the following definition:

(1) The numbers of maxima and zero-crossing must equal to each other or differ at most by one;

(2) At each point of the time series, the mean value between the envelope defined by the local maxima and the envelope defined by local minima should equal 0.

The concrete steps of EMD method are listed as follows:

Step 1 Search all the local extrema of the signals x(t), and connect the local maxima by a cubic spline line to form the upper envelope; accordingly, the local minima is connected to form the lower envelope too.

Step 2 Designate $m_{11}(t)$ as the mean of the upper envelope and the lower envelope, and the difference $h_{11}(t)$ between x(t) and $m_{11}(t)$ can be calculated by the following equation:

$$h_{11}(t)=x(t)-m_{11}(t) \tag{1}$$

If $h_{11}(t)$ satisfies the definition of IMF, $h_{11}(t)$ is the first IMF component of the signals, then go to **step 4** directly, or else go to step 3.

Step 3 If $h_{11}(t)$ does not satisfy IMF definition, then treat $h_{11}(t)$ as the original signals and repeat **step 1** to generate the upper envelop and the lower envelop. Accordingly, the difference $h_{12}(t)$ can be acquired by the following equation:

$$h_{12}(t)=h_{11}(t)-m_{12}(t) \tag{2}$$

where, $m_{12}(t)$ is the mean between the new upper envelop and the lower envelop. If $h_{12}(t)$ satisfies the IMF definition, $h_{12}(t)$ is IMF1, or else repeat **steps 1-3** for k-step till $h_{1k}(t)$ meets the IMF definition.

Step 4 Let $c_1(t)=h_{1k}(t)$, $r_1(t)=X(t)-c_1(t)$, treat $r_1(t)$ as the original signals and repeat **steps 1-3** to generate IMF2.

Step 5 Repeat **steps 1-4** for *n*-step till no more IMF can be extracted from $r_n(t)$.

The original signals x(t) can be decomposed as the sum of IMF1~n and $r_n(t)$:

$$x(t)=\sum_{i=1}^{n} c_i(t)+r_n(t) \tag{3}$$

In fact, the terminal condition that no more IMF can be extracted from $r_n(t)$ is difficult to judge directly, so the standard deviation is introduced:

$$SD=\sum_{t=0}^{T}\frac{[h_{1(k-1)}(t)-h_{1k}(t)]^2}{h_{1(k-1)}^2(t)} \tag{4}$$

where, SD<0.3 can be chosen as the new terminal condition.

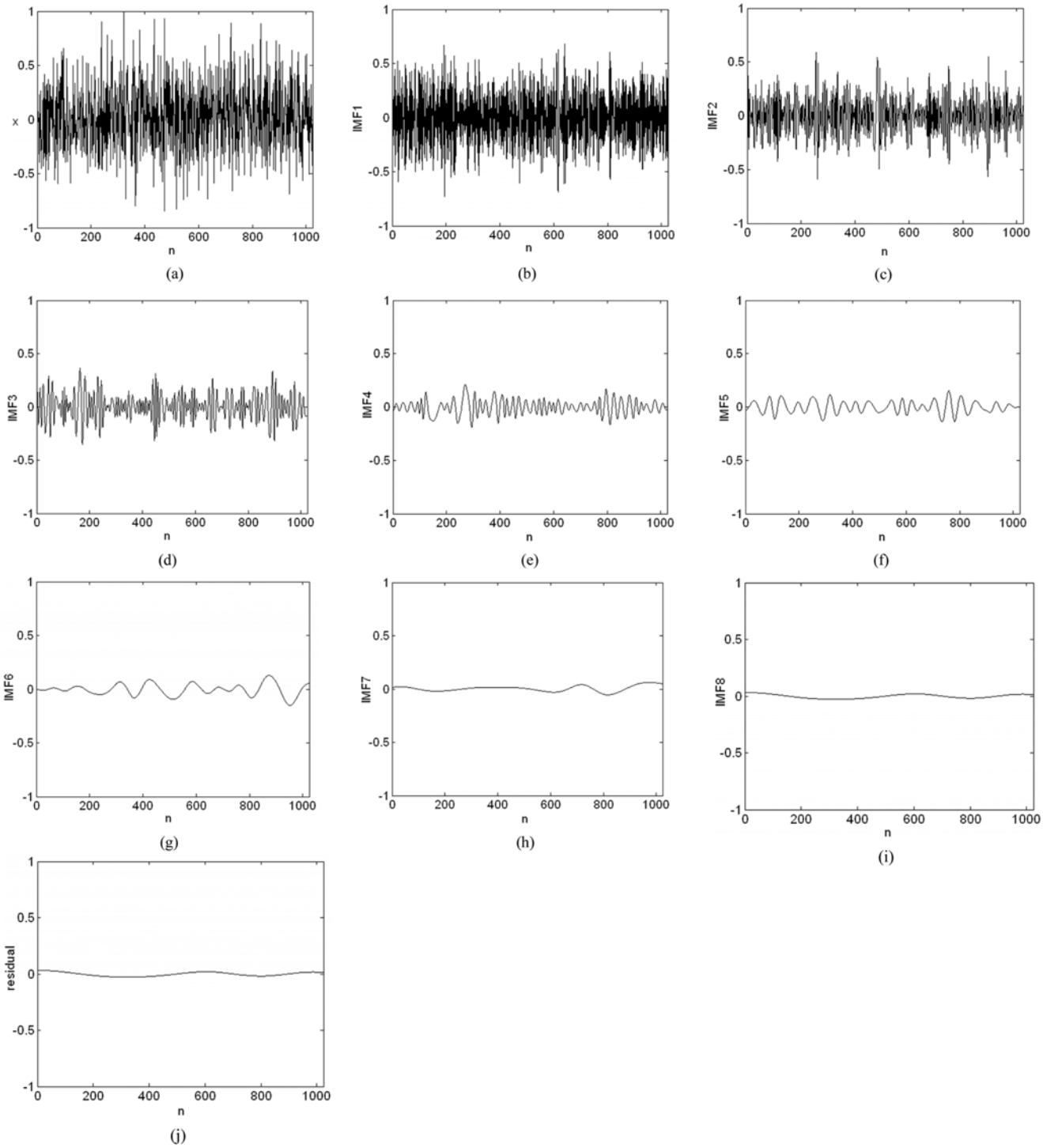

Fig. 2. IMFs of the pressure fluctuation signal: (a) original signals; (b) IMF1; (c) IMF2; (d) IMF3; (e) IMF 4; (f) IMF 5; (g) IMF 6; (h) IMF7; (i) IMF 8; (j) residual.

Take a group of the pressure fluctuation signals, which are normalized and shown in Fig. 2(a) as example. These signals can be decomposed into eight IMF components and one residual r(t), which are shown in Fig. 2(b)-(j).

2. Hilbert Transformation

Hilbert transformation of each IMF component $c_i(t)$ can be acquired by the following equation:

$$H(c_i(t)) = \frac{1}{\pi}\int_{-\infty}^{\infty} \frac{c_i(\tau)}{t-\tau} d\tau \tag{5}$$

A complex conjugate pair that defines an analytic signal, $z_i(t)$, can be formed by $H(c_i(t))$ and $c_i(t)$:

$$z_i(t) = c_i(t) + jH(c_i(t)) = a_i(t)e^{i\theta_i(t)} \tag{6}$$

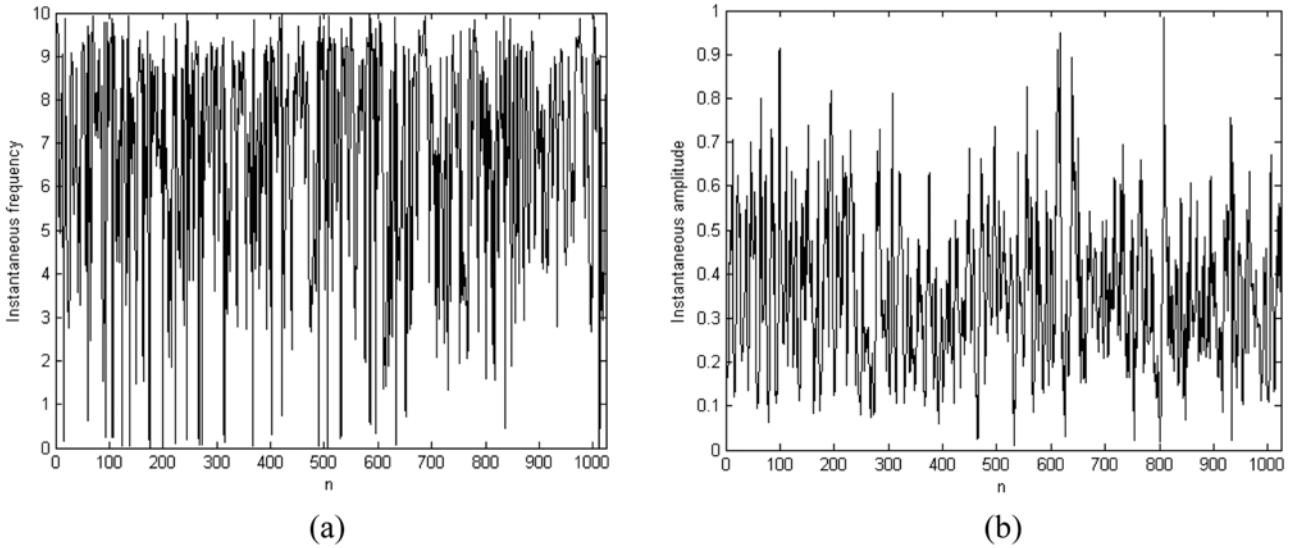

Fig. 3. Hilbert Transformation of IMF1 (a) Instantaneous amplitude; (b) Instantaneous frequency.

where, the instantaneous amplitude $a_i(t)$ and the phases $\theta_i(t)$ can be expressed as follows:

$$a_i(t)=\sqrt{c_i(t)^2+H(c_i(t))^2} \tag{7}$$

$$\theta_i(t)=\arctan\left(\frac{H(c_i(t))}{c_i(t)}\right) \tag{8}$$

Define instantaneous frequency, $w_i(t)$, as:

$$w_i(t)=\frac{d\theta_i(t)}{dt} \tag{9}$$

Accordingly, the original signals x(t) can be expressed as follows:

$$x(t)=Re\left(\sum_{i=1}^{n}a_i(t)e^{j\int w_i(t)dt}\right) \tag{10}$$

Take IMF1 component of the pressure fluctuation signals as example, the instantaneous frequency and amplitude is shown in Fig. 3.

In this paper, energy of the first seven IMF components is extracted from the pressure fluctuation signals to be regarded as eigenvector. The energy of the *i*th component can be calculated by the following equation:

$$E_i=\frac{\sum_{n=1}^{N}|a_i(n)^2|}{N} \tag{11}$$

INTELLIGENT RECOGNITION SYSTEM OF THE FLOW REGIMES IN THE SPOUTED BED

1. RBF Neural Network

Define $X=(x_1, x_2, .., x_n)$ as the input vector of RBF neural network, and $Y=(y_1, y_2, ..., y_n)$ as the actual output vector of RBF neural network. Gaussian function is chosen as the basis function in the hidden layers:

$$\phi_i(x)=\exp(-|X-C_i|^2/2\delta_i^2) \tag{12}$$

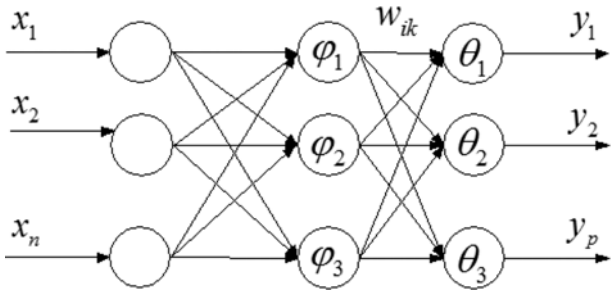

Fig. 4. Structure of RBF neural network.

where, C_i and δ_i represents the center and the extended constant of the *i*th basis function respectively [23-25].

The structure of the RBF neural network is shown in Fig. 4. The nonlinear mapping $X\rightarrow\varphi_i(x)$ has been realized in the input layer, and the linear mapping $\varphi_i\rightarrow y_k$ has been realized in the output layer. The output of the *k*th node in the output layer can be expressed as follows:

$$y_k=\sum_{i=1}^{m}w_{ik}\phi_i(x)-\theta_k, k=1,2,\ldots,p \tag{13}$$

where, m is the node number in the hidden layer; p is the node number in the output layer; w_{ik} is the connection weight between the ith node in the hidden layer and the kth node in the output layer; $\varphi_i(x)$ is the basis function of the ith node in the hidden layer; θ_k is the threshold of the kth node in the output layer; y_k is the output of the kth node.

During the training phase, if the flow regime is packed bed, the output vector of RBF neural network O={1,0,0,0}; if the flow regime is stable spouting, the output vector is {0, 1, 0, 0}; if the flow regime is bubbly fluidized bed, the output vector is {0, 0, 1, 0}; if the flow regime is slugging bed, the output vector is {0, 0, 0, 1}.

2. Theory of Adaptive Genetic Algorithm

In the RBF neural network, the parameters needed to be optimized are **C**, δ, **w** and θ, and adaptive genetic optimization algorithm [26-28] is applied to optimize the parameters in this paper.

Table 2. Characteristic parameters of the typical flow regimes

Flow regime	IMF1	IMF2	IMF3	IMF4	IMF5	IMF6	IMF7
P	0.3513	0.0452	0.0186	0.0099	0.0034	0.0021	0.0009
S	0.2153	0.0532	0.0242	0.0090	0.0060	0.0044	0.0015
BF	0.1397	0.0456	0.0293	0.0136	0.0064	0.0038	0.0025
SB	0.2470	0.0690	0.0183	0.0136	0.0073	0.0095	0.0029

Table 3. Features of one group of signals

Flow regime	IMF1	IMF2	IMF3	IMF4	IMF5	IMF6	IMF7
S	0.2601	0.0639	0.0488	0.0280	0.0104	0.0081	0.0049

The fitness function is determined as follows:

$$F=\frac{1}{\sum_{i=1}^{n}(y_i-f(x_i)^2)+e} \tag{14}$$

where, y_i is the expected output, $f(x_i)$ is the actual output, and e is a small real number, which is to prevent the situation of zero denominator, here $e=10^{-3}$.

The initial crossover probability and the initial mutation probability are determined by Eqs. (14) and (15):

$$P_c^1=\begin{cases}0.9-0.3(f'-f_{avg})/(f_{max}-f_{avg}), & f\geq f_{avg}\\ 0.9, & \text{else}\end{cases} \tag{15}$$

$$P_m^1=\begin{cases}0.1-0.099(f_{max}-f)/(f_{max}-f_{avg}), & f\geq f_{avg}\\ 0.1, & \text{else}\end{cases} \tag{16}$$

where, f' is larger fitness function value of the cross-two bodies, f is the fitness function value of individual, f_{avg} is the average fitness function value in the samples, and f_{max} is the maximum fitness function value of individual in the samples.

Crossover probability and mutation probability change with the evolutional generation, and their changing rules are as follows:

$$P_c^t=\begin{cases}0.9\times\sqrt{1-(t/t_{max})^2} & P_c^t<0.6\\ 0.6 & \text{else}\end{cases} \tag{17}$$

$$P_m^t=\begin{cases}0.1\times e^{(-\lambda\cdot t/t_{max})} & P_m^t<0.001\\ 0.001 & \text{else}\end{cases} \tag{18}$$

where, t is the genetic algebra, t_{max} is the terminated genetic algebra and λ is a constant, here $\lambda=10$.

3. Structure of the Intelligent Recognition System

The recognition system can be divided into three steps: (1) one group of the pressure fluctuation signals is sampled from the spouted bed; (2) EMD is applied to decompose the normalized signals, and HT is applied to transform the IMF components from the time domain into the frequency domain; (3) characteristic parameters are extracted and used as the input vector of the RBF neural network; (3) the flow regimes in the spouted bed can be determined by observing the output of RBF neural network.

4. Optimization of the Parameters in the Intelligent System

There are two factors that may lead to the failure of intelligent model [29]: (1) 'over-fitting' issue (the objective function can reduce to a very low value during the training phase, but the testing error is relatively large); (2) 'under-fitting' issue (the objective function cannot reduce to a low value during the training phase). For solving these issues, 'cross-validation' method [30] is introduced.

The basic steps of 'cross-validation' are listed as follows:

Step. 1 Divide the training samples into n subsamples, and set i=1;

Step. 2 Regard the *i*th subsamples as the testing samples, and the others as the training samples;

Step. 3 Optimize the parameters based on the new training samples by adaptive genetic algorithm.

Step. 4 i=i+1, and repeat Step. 1-3 till i=n

Finally, $\mathbf{w}=\sum\mathbf{w}_i/n$, $\mathbf{C}=\sum\mathbf{C}_i/n$, $\delta=\sum\delta_i/n$, $\mathbf{w}=\sum\mathbf{w}_i/_n$, and $\theta=\sum\theta/n$.

The characteristic parameters of the typical flow regimes in Fig. 1 are shown in Table 2.

Let the subsample size=75, the input node number=7, the hidden node number=13, the output node number=4, the population size N_i=40, the maximum genetic algebra M_a=500 and the binary digit of each variable P_r=20. After the optimization process, the relative error can be reduced to about 1.5%.

5. Examination of the Performance of the Intelligent System

Eighty groups of pressure fluctuation signals (twenty groups in the packed bed, twenty groups in the spouted spouting bed, twenty groups in the bubbling fluidized bed and twenty groups in the slugging bed) are selected as testing samples. Only one group of signals in the spouted bed, which are shown in Table 3, is analyzed in detail here.

The input vector of RBF is {0.2601, 0.0639, 0.0488, 0.0280, 0.0104, 0.0081, 0.0049} and the output vector of RBF is {0.0901, 0.8557, 0.0777, 0.0215}. The second component of the output vector is the largest, so the flow regime is stable spouting, which is consistent with the observation result.

The recognition accuracies of the flow regimes in spouted bed are shown in Table 4.

Table 4. Recognition accuracy of different flow regimes

Flow regime	Packed bed	Stable spouting	Bubbly fluidized bed	Slugging bed
Recognition accuracy	90%	85%	85%	95%

CONCLUSIONS

To break the limitation of the classical time-frequency analysis methods, HHT has been applied to extract the features from the pressure fluctuation signals in the spouted bed: first, the pressure fluctuation signals were decomposed into eight IMF components, and then Hilbert transformation was used to transform IMF component from the time domain into the frequency domain.

Based on HHT analysis, the flow regimes have been recognized by RBF neural network, and adaptive genetic algorithm has been used to optimize the parameters in RBF neural network. The recognition accuracies of packed bed, spouted bed, bubbling fluidized bed and slugging bed can reach 90%, 85%, 85%, 95% respectively.

ACKNOWLEDGEMENTS

The authors thank the National Basic Research Program of China (2007CB210208) and the program sponsored for scientific innovation research of college graduate in Jangsu province (CX10B_065Z) for financial support.

REFERENCES

1. L. A. P. Freitas, O. M. Dogan, C. J. Lim, J. R. Grace and B. Luo, *Chem. Eng. Commun.*, **181**, 243 (2000).
2. L. A. P. Freitas, O. M. Dogan, C. J. Lim, J. R. Grace and D. R. Bai, *The Canadian J. Chem. Eng.*, **82**, 60 (2004).
3. S. Lin and P. A. Kew, *Experimental Heat Transfer.*, **14**, 135 (2001).
4. B. Leckner, G. I. Palchonok and F. Johnsson, *Thermal Sci.*, **6** (2002).
5. G. Chaplin, T. Pugsley and C. Winters, *Powder Technol.*, **142**, 110 (2004).
6. J. Xu, X. J. Bao, W. S. Wei, S. K. Shen, H. T. Bi, J. R. Grace and J. C. Lim, *Canadian J.Chem. Eng.*, **82**, 37 (2004).
7. J. Xu, X. J. Bao, W. S. Wei, J. R. Grace and J. C. Lim, *Ind. Eng. Chem. Res.*, **43**, 5754 (2004).
8. J. Xu, X. J. Bao, W. S. Wei, S. Gang, S. K. Shen, H. T. Bi, J. R. Grace and J. C. Lim, *Powder Technol.*, **141**, 142 (2004).
9. W. Q. Zhong and M. Y. Zhang, *Powder Technol.*, **159**, 121 (2005).
10. W. Q. Zhong and M. Y. Zhang, *Powder Technol.*, **152**, 52 (2005).
11. W. Q. Zhong, X. F. Wang, Q. J. Li, B. S. Jin, M. Y. Zhang, R. Xiao and Y. J. Huang, *Canadian J. Chem. Eng.*, **87**, 221 (2009).
12. E. Piskova and L. Morl, *Chem. Eng. Sci.*, **63**, 2307 (2008).
13. N. E. Huang, Z. Shen, S. R. Long, M. C. Wu, H. H. Shih and Q. Zheng, *Proceedings of the Royal Society of London A*, **454**, 903 (1998).
14. N. E. Huang, Z. Shen and S. R. Long, *Annual Review of Fluid Mechanics*, **31**, 417 (1999).
15. N. E. Huang, M. C. Wu, S. R. Long, S. P. Shen, W. Qu and P. Gloersen, *Proceedings of the Royal Society of London A*, **459**, 2317 (2003).
16. N. E. Huang. *The Hilbert-Huang transform in engineering,* Boca Raton, FL, CRC Press (2005).
17. P. A. Hwang, N. E. Huang and D. W. Wang, *Appl. Ocean Res.*, **25**, 187 (2003).
18. D. Marcus and T. Schlurmann. *Ocean Engineering,* **31**, 1783 (2004).
19. B. Sun, H. J. Zhang, C. Lu and Y. X. Zhao, *Chinese J. Chem. Eng.*, **14**, 24 (2006).
20. D. J. Yu, J. S. Cheng and Y. Yang. *Mech. Syst. Sign. Process.*, **19**, 259 (2005).
21. Y. J. Li, P. W. Tse, X. Yang and J. G. Yang. *Mech. Syst. Sign. Process.*, **24**,19 (2010).
22. W. Q. Zhong and M. Y. Zhang, *Proceedings of CSEE*, **25**, 13 (2005).
23. D. R. Hush and B. G. Horne, *IEEE Sign. Process.*, **10**, 8 (1993).
24. M. Bianchini, P. Frasconi and M. Gori. *IEEE Transaction Neural Networks*, **6**, 749 (1995).
25. A. S. Zhang and L. Zhang, *Comput. Struct.*, **82**, 2333 (2004).
26. Z. Bingul, *Applied Soft Computing*, **7**, 791 (2007).
27. F. T. S. Chan, S. H. Chung and P. L. Y. Chan, *Expert Systems with Applications*, **29**, 364 (2005).
28. Q. H. Wu, Y. J. Cao and J. Y. Wen, *Int. J. Electrical Power & Energy Systems*, **20**, 563 (1998).
29. S. J. An, W. Q. Liu and S. Venkatesh, *Pattern Recognition*, **40**, 2154 (2007).
30. R. Deng, Y. J. Ma and Y. M. Liu, *J. Tianjin Univ. Sci. Technol.*, **22**, 58 (2007).